

# A numerical study of hydrogen inhibition of char gasification using detailed heterogeneous and homogeneous chemical kinetics

Joanna Lazar,<sup>†,‡</sup> Nils Erland L. Haugen,<sup>\*,§,‡</sup> Jonas Kruger,<sup>‡</sup> and Andrzej Szlek<sup>†</sup>

*Silesian University of Technology, Konarskiego 22, 44-100 Gliwice, Poland, Norwegian University of Science and Technology, 7491 Trondheim, Norway, and SINTEF Energy Research, 7465 Trondheim, Norway*

E-mail: nils.e.haugen@sintef.no

## Abstract

It has been known for a long time that hydrogen in the gas phase tends to inhibit gasification of char at low and intermediate temperatures. At higher temperatures, however, there are indications that hydrogen may speed up gasification. The mechanisms behind these effects are currently not understood. In this work, a newly developed detailed chemical kinetics model for char has been used in order to study the mechanisms behind the hydrogen inhibition and speed-up of char gasification. For conditions assumed in this work, the hydrogen inhibition is found for  $T < 2000$  K, while for  $T > 2000$  K the hydrogen in the gas phase speeds up the char conversion. By studying

---

\*To whom correspondence should be addressed

<sup>†</sup>Silesian

<sup>‡</sup>NTNU

<sup>§</sup>SINTEF

the species reaction rates together with the individual rate of every heterogeneous reaction, the reasons for hydrogen influence on char gasification are attempted explained for a wide range of different temperatures in this paper. The focus is not on investigating a real gasifier, but rather to understand the fundamental mechanism behind hydrogen inhibition of char.

## Introduction

For many applications it is not feasible, or just not economical, to use solid fuels directly. It is therefore often useful to convert the solid fuel to either a gaseous or a liquid fuel before it is used. Solid fuels, such as e.g. coal, biomass or pet coke, can be converted to a synthesis gas (syngas) through reactions with oxygen, steam or carbon dioxide in a gasifier. The syngas can then be used for e.g. electricity production in an Integrated Gasification Combined Cycle (IGCC), for production of liquid fuels for the transportation sector or for production of hydrogen for fuel cells or use in the chemical industry.

The newly developed detailed heterogeneous chemical kinetics model of Tilghman & Mitchell,<sup>1</sup> with 18 reversible reactions for char reactions with oxygen, steam and carbon dioxide, has been used in the current work. Hecht et al. (2011)<sup>2</sup> have shown that in oxygen fired systems, it is important to include the effects of CO<sub>2</sub> gasification. The chemical mechanism is used in order to study the mechanism behind the hydrogen inhibition of char gasification at low and intermediate temperatures. The effect of a speed-up of the gasification process at higher temperatures has also been studied. In order to check the impact of hydrogen on the char gasification, without changing the thermodynamics of the fluid, the heterogeneous reactions that have gaseous molecular hydrogen as a reactant are turned on and off. I.e.; the impact of a given reaction where hydrogen is a reactant is investigated by comparing the results obtained when that specific reaction is turned off with the results obtained when all reactions are turned on. In this way the impact of the hydrogen on the gasification process can be studied in great detail. The respective reactions are turned off by setting their pre-exponential factors to zero.

For low temperatures or small char particles, the conversion rate is kinetically controlled and the pore surface of the entire particle volume is reacting. This, which is known as Zone I conversion, yields a constant particle radius, where the particle mass is reduced by a decrease in density. For very high temperatures or large particles, the reactants are consumed at the external surface of the particles. This decreases the particle radius while keeping the density constant, and is known as Zone III conversion. Zone II conversion, on the other hand, is observed for intermediate temperatures and particle sizes. For this regime, both particle radius and density is decreased and the relative fraction of decrease is described by Haugen et al. (2014).<sup>3</sup>

The effect of hydrogen inhibition on surface reactions was also recently studied by Pineda & Chen.<sup>4</sup> Here the authors use a heterogeneous reaction mechanism consisting of 8 reaction steps in a perfectly stirred reactor to find that the inhibition of hydrogen is due to the adsorbed molecular hydrogen filling up a significant fraction of all the free sites on the carbon surface.

Hydrogen inhibition has previously been studied under many different gasifying conditions. One of the earlier discussions on the reaction mechanism behind hydrogen inhibition is found in Laurendeau (1978).<sup>5</sup> In previous experimental work, inhibition has been observed at low (1 atm) and moderate (10 atm) steam pressures and moderate temperatures (950 -1250 K),<sup>6-10</sup> as well as at high pressures (40 - 50 atm).<sup>11,12</sup> gasification of a natural graphite at temperatures between 960 °C and 1120 °C and low pressures, Biederman et al.<sup>8</sup> found that hydrogen inhibition was caused by dissociative chemisorption of hydrogen on active carbon sites. For graphite- $CO_2$  reactions, they found that the inhibition was due to hydrogen chemisorbing on impurity catalyst sites. Barrio et al. studied the steam gasification of wood at atmospheric pressure and in the temperature range from 750 °C to 950 °C.<sup>10</sup> In their work it is concluded that the hydrogen inhibition effect can be described on the basis of Langmuir-Hinshelwood kinetics. The aim of the work of Tay et al.<sup>13</sup> was to investigate the role of hydrogen during the gasification of a Victorian brown coal at 800 °C in a fluidised-bed/fixed-bed reactor. Here it was found that the inhibiting effects of hydrogen were not limited to its chemisorption on the char surface. The presence of hydrogen also changed the aromatic structure of char during gasification, which is most likely due to the ability of hydrogen

radicals to penetrate into the char matrix. In the work of Fushimi et al.<sup>14</sup> on steam gasification of woody biomass char, it was observed that hydrogen inhibition was due to reverse oxygen exchange reactions in the first period and dissociative hydrogen adsorption on the char particle in the second period.

In the current work, the focus is on gasification of char from Wyodak coal, which is a sub-bituminous coal from Wyoming, USA. It is expected, however, that the results should also be similar for other fuels, such as e.g. other coal qualities or biomass.

## Model description

In this section the essentials of the numerical model used to simulate the char gasification are described. The implementation of the numerical model has been verified by Haugen, Tilghman and Mitchell (2014)<sup>3</sup> against the particle resolved simulation tool (DNS) of the Stanford group. For more information on the model, the reader is referred to Haugen, Mitchell and Tilghman (2015).<sup>15</sup>

In the following, particles are assumed to be spherical and uniform in composition and morphology, while the ash is uniformly distributed throughout the particle volume. In addition, ash in the char can not react or be evaporated, and there is no exchange of mineral matter between the particle and the gas phase.

The calculations are made on a single particle in the particle cloud. It is assumed that all other particles behave in the same way as the considered one. The carbon in the particle will react with the hot reactive gases ( $O_2$ ,  $H_2O$  and  $CO_2$ ), causing the mass, apparent density and size of the particle to change with time. The heterogeneous chemical kinetics were developed by Tilghman & Mitchell<sup>1</sup> based on the work of Haynes (2001),<sup>16</sup> and is presented in Table 1, while the homogeneous chemical kinetic mechanism used is the GRI-mech 3.0.<sup>17</sup> The ultimate and proximate analysis of the coal are presented in Table 2 and Table 3. In the heterogeneous reaction scheme, the adsorbed species  $C(H)$ ,  $C(O)$ ,  $C(CO)$ ,  $C(OH)$  represent a hydrogen atom, oxygen atom, carbon monoxide

and  $OH$  group adsorbed on a carbon site, respectively, while  $C_2(O_2)$  represent two adjacent carbon sites that have adsorbed one oxygen atom each. The bulk carbon site,  $C_b$ , is a carbon atom bonded to four other carbon atoms. As a result of chemical reactions, the bulk carbon site can become a free carbon site. The free carbon site,  $C_f$ , is a carbon atom that is available for adsorption of gas phase species. Due to the particle-to-gas reactions, the oxygen, carbon and hydrogen compounds desorb from the carbonaceous matrix and leave the particle surface. As a result of this process, an underlying carbon atom becomes a free carbon site.

Table 1: The intrinsic heterogeneous reaction mechanism. The units of both the activation energy  $E_k$  and the distribution width  $\sigma_k$  is kJ/mol, while the units of  $A_k$  is such that the units of  $R_{\text{reac},c}$  in Eq. (9). is mol/m<sup>2</sup>/s.

Nr.	Reaction	$A_k$	$E_k$	$\sigma_k$
R1	$2C_f + H_2O \leftrightarrow C(OH) + C(H)$	$2.1 \times 10^6$	105	0
R2	$C(OH) + C_f \leftrightarrow C(O) + C(H)$	$4.1 \times 10^{11}$	80	0
R3	$C(H) + C(H) \leftrightarrow H_2 + 2C_f$	$1.4 \times 10^{11}$	67	0
R4	$C(O) + C_b \rightarrow CO + C_f$	$1.0 \times 10^{13}$	353	28
R5	$C(OH) + C_b \leftrightarrow HCO + C_f$	$1.0 \times 10^{13}$	393	28
R6	$C_b + C_f + C(H) + H_2O \leftrightarrow CH_3 + C(O) + C_f$	$1.0 \times 10^{13}$	300	0
R7	$C_b + C_f + C(H) + H_2 \leftrightarrow CH_3 + 2C_f$	$1.0 \times 10^{13}$	300	0
R8	$C_f + C(H) + CO \rightarrow HCO + 2C_f$	$1.0 \times 10^{13}$	300	0
R9	$C(H) + C(H) \rightarrow CH_2 + C_f$	$3.0 \times 10^{11}$	426	0
R10	$CO_2 + C_f \leftrightarrow C(O) + CO$	$3.7 \times 10^3$	161	0
R11	$C_b + CO_2 + C(O) \rightarrow 2CO + C_f$	$1.26 \times 10^8$	276	0
R12	$C(CO) \leftrightarrow CO + C_f$	$1.0 \times 10^{13}$	455	53
R13	$CO + C(CO) \rightarrow CO_2 + 2C_f$	$9.8 \times 10^6$	270	0
R14	$2C_f + O_2 \rightarrow C(O) + CO$	$5.0 \times 10^{10}$	150	0
R15	$2C_f + O_2 \rightarrow C_2(O_2)$	$4.0 \times 10^7$	93	0
R16	$C_f + C_b + C(O) + O_2 \rightarrow CO_2 + C(O) + C_f$	$1.5 \times 10^7$	78	0
R17	$C_f + C_b + C(O) + O_2 \rightarrow CO + 2C(O)$	$2.1 \times 10^7$	103	0
R18	$C_b + C_2(O_2) \rightarrow CO_2 + 2C_f$	$1.0 \times 10^{13}$	304	33

Arrhenius parameters shown in Table 1 were obtained for Wyodak coal<sup>1</sup> based on Thermogravimetric analysis (TGA). The obtained activation energies were found to be within expected ranges when compared with values for chars and activated carbon from the literature. In the experiments, the char conversion was limited only by the chemical reaction rates, i.e.; the experiments

Table 2: Proximate analysis of Wyodak coal.

Property	amount (wt-%)
fixed carbon	35.06
volatile matter	33.06
moisture	26.30
ash	5.58

Table 3: Ultimate analysis of Wyodak coal.

Property	amount (wt-%)
carbon	69.8
hydrogen	5.65
oxygen (diff)	15.6
nitrogen	0.94
total sulfur	0.43
ash	7.57

where kinetically controlled. The pressure was held at 1 atm and the testing temperatures were selected according to the reacting gases: 700 - 900 °C for environments containing  $H_2O$ , 800 - 1000 °C for environments containing  $CO_2$  and 400 - 550 °C for environments containing  $O_2$ . The char specific surface area was measured with the BET method. Since the heterogeneous reaction mechanism is intrinsic, the surface area is required in order to calculate the total reaction rate of the char particle.

In this paper, the focus is on the two reactions that have molecular hydrogen as a reactant. This corresponds to reaction R3 backward (R3b) and reaction R7 forward (R7f). Hydrogen inhibition of char gasification is studied by investigating the effect of de-activating these two reactions.

The exchange of matter between the particles and the ambient gas is caused by reactions between the gas and the solid phase. The species production rate can be symbolized by  $\omega_{pg,i}$  for the particle-to-gas reactions and  $\omega_{gg,i}$  for the gas-to-gas reactions. These two terms determine the change of the mass fraction of species  $i$  in the gas phase.

## Governing gas phase equations

In the following a brief overview of the most important equations will be presented. For a full description of all relevant equations, the reader is referred to Haugen et al.<sup>15</sup>

The gas phase is defined by three governing equations describing the evolution of mass, species and temperature in the gas phase. The first equation describes the evolution of the mass of the gas phase  $m_g$ ;

$$\frac{dm_g}{dt} = \frac{m_g}{\rho_g} \sum_{i=1}^{N_{s,gas}} \omega_{pg,i} M_i, \quad (1)$$

where  $\rho_g$  is the mass density of the gas phase,  $M_i$  is the molar mass of species  $i$  and  $\omega_{pg,i}$  is the molar production rate of species  $i$  due to reactions between the solid and the gas phase (heterogeneous reactions). The second equation describes the mass fraction  $Y_i$  of species  $i$  in the gas phase;

$$\rho_g \frac{dY_i}{dt} + Y_i \sum_{k=1}^{N_{s,gas}} \omega_{pg,k} M_k = (\omega_{gg,i} + \omega_{pg,i}) M_i, \quad (2)$$

where  $\omega_{gg,i}$  is the molar production rate of species  $i$  due to gas phase (homogeneous) reactions. The third equation is the energy equation, which is here represented by the temperature;

$$\rho_g c_{p,g} \frac{dT_g}{dt} + \sum_{i=1}^{N_{s,gas}} h_i (\omega_{gg,i} + \omega_{pg,i}) M_i = n_p (Q_h + Q_c), \quad (3)$$

where  $c_{p,g}$  is the heat capacity of the gas mixture at constant pressure,  $T_g$  is the temperature of the gas,  $h_i$  is the enthalpy of species  $i$ ,  $Q_h$  is the energy transfer from the solid phase to the gas phase due to heterogeneous reactions and  $Q_c$  is the heat transfer from the particle to the gas mixture due to convection and conduction.

## Governing solid phase equations

In this subsection, the governing equations describing mass transport and chemical reactions in the solid phase (the char) are presented.

## Particle mass

The evolution of the carbonaceous part of the char particle mass  $m_c$  is described by

$$\frac{dm_c}{dt} = -S_t M_c R_{\text{reac},c}, \quad (4)$$

where  $M_c$  is the molar mass of carbon and  $R_{\text{reac},c}$  is the molar reaction rate of carbon. Since the heterogeneous reaction mechanism is intrinsic, the total surface area of the carbonaceous part of the particle,  $S_t$ , is required. This is in contrast to for apparent reaction mechanisms where the effect of the surface area is implicitly included in the reaction kinetics.

## Particle temperature

The temperature evolution of the char particle is given by

$$\frac{dT_p}{dt} = \frac{1}{m_p c_{p,p}} (Q_{\text{reac}} - Q_c + Q_{\text{rad}}), \quad (5)$$

where  $T_p$  is the particle temperature,  $c_{p,p}$  is the specific heat capacity of the particle,  $Q_{\text{reac}}$  is the heating due to heterogeneous reaction,  $Q_c$  is the heat transfer from the char particle to the gas phase via convection and conduction and  $Q_{\text{rad}}$  is the heating due to radiation.<sup>18</sup>

## Adsorbed species

The number of moles of adsorbed species  $j$  is given by

$$N_j = C_{s,j} S_t, \quad (6)$$

where  $C_{s,j}$  is the concentration of adsorbed species  $j$  on the surface of the char particle. The rate of change in the site fraction of adsorbed species  $j$  is given by

$$\frac{d\Theta_j}{dt} = \frac{R_{\text{spec},j}}{\xi_n} + A R_{\text{reac},c} \Theta_j, \quad (7)$$



where  $\Theta_j = C_{s,j}/\xi_n$  is the adsorbed species site fraction and  $\xi_n$  is the total surface concentration of carbon sites (both free and occupied). The molar rate of adsorbed species production is given by  $R_{spec,j}$  while  $A$  is an active surface area<sup>15</sup>

## Species concentrations at the particle surface

The relationship between the flux of gas phase species  $i$  through the boundary layer to the external particle surface and the net production of species  $i$  via particle-to-gas reactions, in steady state, is given by

$$\dot{n}_i - X_{i,s}\dot{n}_{total} = -k_{im}(X_{i,\infty} - X_{i,s}), \quad (8)$$

where  $X_{i,\infty}$  is the mole fraction of species  $i$  in the ambient gas phase and  $X_{i,s}$  is the mole fraction of species  $i$  at the particle surface. The species mass transfer coefficient is represented by  $k_{im}$ . The molar flux of species  $i$ ,  $\dot{n}_i$ , is defined as positive in the direction away from the particle surface, such that the total molar flux away from the particle is given by  $\dot{n}_{total} = \sum \dot{n}_i$ . A Newton method is used to solve Eq. (8).

## Internal particle burning and the effectiveness factor

The molar rate of reaction  $k$  is given by

$$R_{reac,k} = k_k \prod_{i=1}^{N_{s,gas}+N_{s,ads}} C_i^{\nu_{i,k}}, \quad (9)$$

where  $k_k$  is the rate coefficient of reaction  $k$ . The concentration of species  $i$  is represented by  $C_i$  while  $\nu_{i,k}$  is the Stoichiometric coefficient. This equation is valid when the concentration of reactants of reaction  $k$  inside the particle is uniform. In a situation where the mass transport rates are slower than the chemical reaction rates, the gas does not penetrate the particle completely. As a result, the concentration of reactants inside the particle is not uniform and the rate of reaction  $k$

is lower than what is found from Eq. (9). The reduced rate of reaction  $k$  can be written as

$$R_{\text{reac},k} = \eta_k k_k \prod_{i=1}^{N_{s,\text{gas}}+N_{s,\text{ads}}} C_i^{v_{i,k}}, \quad (10)$$

where

$$\eta_k = \frac{3}{\phi} \left[ \frac{1}{\tanh(\phi)} - \frac{1}{\phi} \right] \quad (11)$$

is the effectiveness factor of reaction  $k$  and  $\phi$  is the Thiele modulus.<sup>19</sup>

The evolution of the particle radius vs. density is also handled based on the effectiveness factor, as described in Haugen et al. (2014).<sup>3</sup>

## Results

In order to investigate the effect of molecular hydrogen in the gas phase on the heterogeneous reactions, the heterogeneous reactions containing molecular hydrogen as a reactant is either activated or de-activated. The reactions are de-activated by setting their reaction rates to zero. All other conditions are kept unchanged. The first relevant reaction is the reverse part of reaction R3, which in the following is referred to as R3b:



where two free carbon sites on the particle surface and a hydrogen molecule reacting to become two adjacent carbon sites that each have an adsorbed hydrogen atom. The other relevant reaction is the forward part of reaction R7 (R7f):



where the free carbon site adsorbs the hydrogen molecule from the gas phase. During the process of reaction, the hydrogen molecule moves, binds to the hydrogen atom adsorbed on the carbon

Table 4: Studied cases A, B, C and D. Reactions R3b,  $H_2 + 2C_f \rightarrow C(H) + C(H)$ , and reaction R7f,  $C_b + C_f + C(H) + H_2 \rightarrow CH_3 + 2C_f$ , are simulated to be active or not active.

Case	R3b	R7f
Case A	ON	ON
Case B	OFF	ON
Case C	ON	OFF
Case D	OFF	OFF

site  $C(H)$  and desorbs and leaves the particle as  $CH_3$ . An underlying bulk carbon becomes a free carbon site.

By turning on and off reactions R3b and R7f, four different test cases can be defined, as presented in Table 4. The purpose of this paper is to investigate the impact of  $H_2$  in the gas phase on the time that is needed to reach full conversion of the char particle, and to understand the reasons of this impact. It is assumed that full conversion of a particle is reached when 99% of the solid carbon has been converted.

In the following the impact of the hydrogen in the gas phase on char gasification at low, intermediate and high temperatures is studied. It is assumed that the temperatures of the fluid and the particles inside the reactor during the conversion process is constant. Small char particles, with Stokes numbers less than unity are used. Furthermore, the reactor is assumed to be perfectly stirred within a small sub-volume following the particles, such that both species and particles are homogeneously distributed within this sub-volume. This means that the char particles stay within the fluid element into which they were injected throughout the course of conversion. As such, the process can be thought of as a batch process for each particle, even though the reactor itself is continuous. The exception from the homogeneity of the simulation domain is the thin boundary layer around each char particle, where gradients in gas phase species exist as described by Eq. (8). It is clear that the assumption of constant gas temperature is not valid in a real application, this assumption is nevertheless made in order to more clearly see the effect of temperature on the reactions and correspondingly also on the amount of hydrogen inhibition.

It should also be noted that in real gasification of coal, the properties of the char will depend on the conditions under which the char was formed. This effect is not account for here, and all char samples have been formed under the same conditions.

Conversion of the char particle exposed to the conditions shown in Table 5 and reacting according to the set of reactions presented in Table 1, describe the base case simulation (Case A). See Table 4 for a description of the other cases (B, C and D).

Table 5: Properties for the simulation at constant temperature inside the reactor.

Property	Value	Unit
Carbon to gas mole ratio	0.5	-
Reactor wall temperature	700	K
Pressure	$2.4 \times 10^6$	Pa
Initial particle radius	$5.0 \times 10^{-5}$	m
Initial particle density	1300	kg/m <sup>3</sup>
Initial mole fraction of $H_2O$	0.50	-
Initial mole fraction of $O_2$	0.45	-
Initial mole fraction of $N_2$	0.05	-

The time to reach full conversion as a function of temperature is shown in Fig. 1. The time to reach full conversion is symbolized by  $\tau$ . At high temperatures ( $T > 1900$  K), it takes less then 1 s to reach full conversion. It can also be seen that in the temperature range 1150 K to 2000 K the full conversion is reached faster for cases B and D than for cases A and C. At low temperatures ( $T < 1400$  K), it can be observed that  $\tau$  is longer for case C than for case A. In the temperature range 2000 K to 2650 K, it takes longer to reach full conversion for cases B and D than for cases A and C. Based on this, it is clear that the impact of the hydrogen on the char gasification strongly depends on the gasification temperature.

Lets now compare the time it takes for the char to reach full conversion in each case, where one of the hydrogen reactions (cases B and C) or both of them (case D) are deactivated, with the time it takes to reach full conversion in base case (case A), in the different temperatures. This relationship can be expressed by the ratio of the time to reach full conversion in cases B, C and D, respectively, to the time to reach full conversion in case A. These ratios are symbolized by  $\alpha$  and can be written

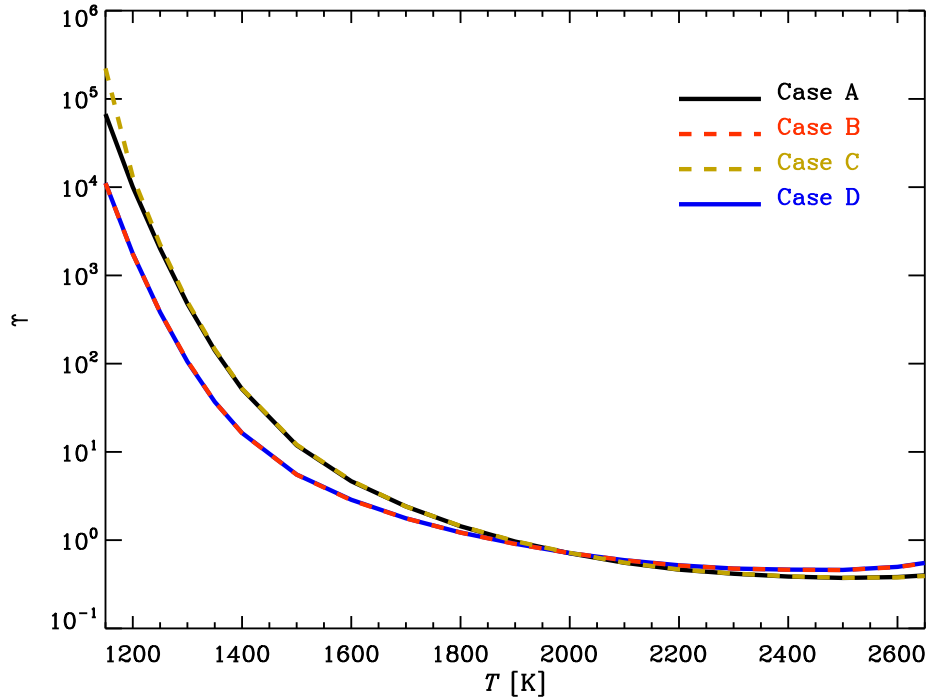


Figure 1: Time to reach full conversion of the char as a function of temperature.

as

$$\alpha_B = \frac{\tau_B}{\tau_A}, \alpha_C = \frac{\tau_C}{\tau_A} \text{ and } \alpha_D = \frac{\tau_D}{\tau_A}, \quad (14)$$

when  $\tau_A$ ,  $\tau_B$ ,  $\tau_C$  and  $\tau_D$  represent the time to reach full conversion in case A, B, C and D, respectively.

In Fig. 2, the relative time to reach full conversion of the char as a function of temperature for cases with (black line) and without (colored lines) hydrogen reactions is shown. It can be seen that  $\alpha_B$  and  $\alpha_D$  increase with increasing temperature, reach unity at about 2000 K and continue to increase. It is also seen that  $\alpha_C$  decreases with increasing temperature, reaches unity at about 1400 K and remains equal to unity at higher temperatures.

By comparing cases A and B, it is seen that hydrogen in the gas phase inhibits char gasification at low and intermediate temperatures ( $T < 2000$  K), while hydrogen speeds up the gasification process at high temperatures ( $T > 2000$  K). By comparing cases B and D it also seems clear

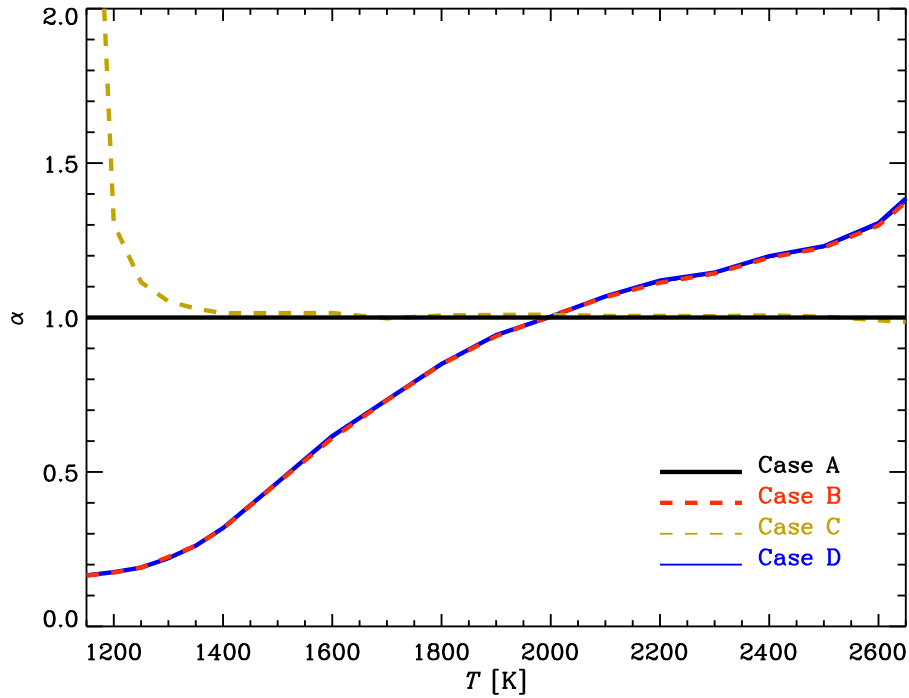


Figure 2: Relative time to reach full conversion of the char as a function of temperature.

that reaction R7f does not have a significant impact on the results, and hence, that the hydrogen inhibition is primarily due to reaction R3b.

In order to study the exact mechanism behind the impact of the hydrogen on char gasification, the gasification process has been studied in detail for three selected temperatures. The lowest temperature (1150 K) corresponds to the lowest temperature for which full conversion could be reached, the intermediate temperature (2000 K) correspond to the temperature where the time to reach full conversion both with and without the hydrogen reactions turned on are equal, while the higher temperature (2650 K) correspond to the highest temperature where a numerical result could be obtained.

The mechanism employed in this work is designed to study the process of gasification at low and intermediate temperatures. However, in this section, the mechanism has been used to simulate char gasification in a much wider temperature range. It will later become evident when studying the species production rates that the heterogeneous mechanism is “unstable” at very high temper-

atures  $\sim 2600$  K. This clearly means that the mechanism can not be fully trusted at these high temperatures. These problems do not, however, seem to have any substantial impact on the overall results. By “unstable” it is meant that the simulation code is not able to identify one single solution, but rather jumps between two neighbouring possible solutions.

### Gasification at 1150 K

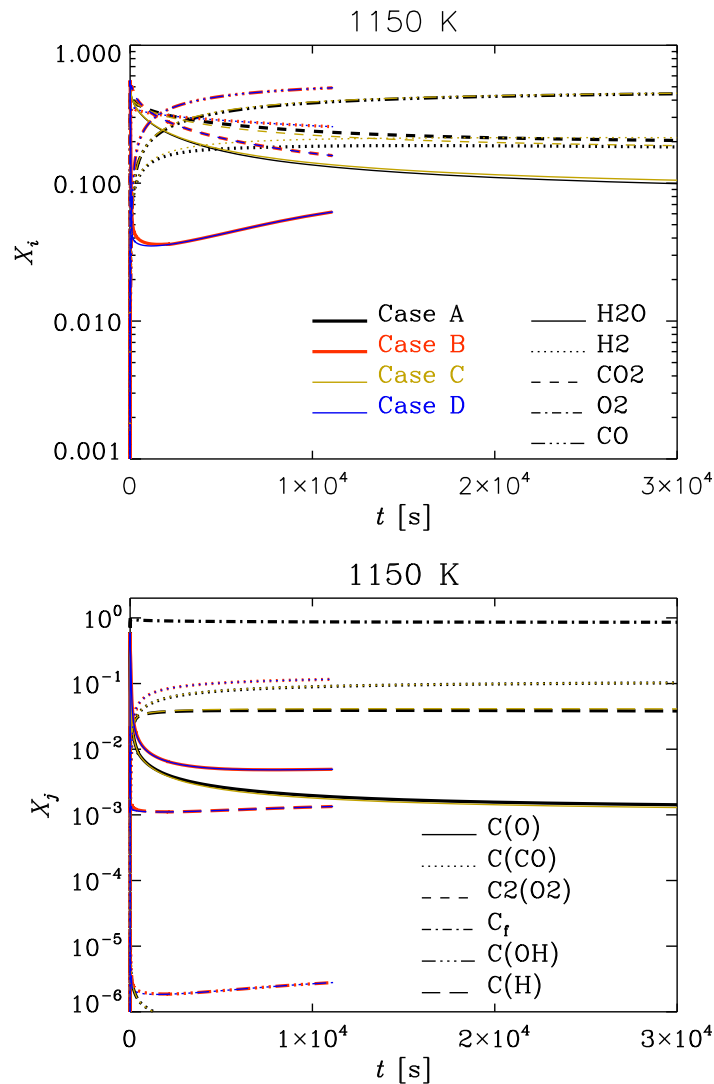


Figure 3: Gas phase species fraction  $X_i$  (top panel) and surface fraction  $X_j$  of adsorbed species (bottom panel) as a function of time at temperature of 1150 K.

At a temperature of 1150 K, turning off reaction R3b slows down the overall production of

$C(H)$ , which is seen by comparing cases A and B in Fig. 3. Since  $C(H)$  is a reactant in reactions R1b,  $2C_f + H_2O \leftrightarrow C(OH) + C(H)$  and R2b,  $C(OH) + C_f \leftrightarrow C(O) + C(H)$ , the molar rate of both reactions R1 and R2 is higher when reaction R3b is de-activated. The net result of this is that more  $C(O)$  is produced, which leads to higher molar rates of reactions R4,  $C(O) + C_b \rightarrow CO + C_f$ , R10b,  $CO_2 + C_f \leftrightarrow C(O) + CO$  and R11  $C_b + CO_2 + C(O) \rightarrow 2CO + C_f$ . In reactions R4 and R11 a carbon atom is removed from the solid surface, and as such, these reactions have a positive impact on the conversion rate of the char. Since reaction R10 is neutral with respect to its impact on the conversion, the increased conversion rate of the char when reaction R3b is turned off is due to the higher amount of adsorbed oxygen on the surface when there is less adsorbed hydrogen present.

When reaction R7f is de-activated, we see from Eq. (2) that the time to reach full conversion increases for very low temperatures. The reason for this is two-fold; first, the de-activation of R7f yields a higher concentration of adsorbed hydrogen, which, as described in the previous paragraph, has a negative effect on the rate of conversion. It can, however, be seen from Fig. 3 that the levels of adsorbed hydrogen and oxygen are rather similar for cases A and C, such that this effect is not expected to be significant. Secondly, since R7f removes one carbon from the solid surface, the de-activation of this reaction will also reduce the rate of conversion directly. This is probably the main reason for the longer times to reach full conversion when reaction R7f is turned off for temperatures less than 1400 K.

## **Gasification at higher temperatures**

In this section the gasification characteristics at temperatures of 2000 K and 2650 K is presented. It should be noted that at these high temperatures, the assumption that the ash can not evaporate is no longer valid.

From Fig. 2 it can be seen that the de-activation of reaction R3b, at a temperature of 2000 K, does not influence the net rate of conversion. The main reason that the de-activation of R3b does not have an effect at this temperature, even though the effect was substantial at 1150 K, is that the de-activation of reaction R3b does no longer have an effect on the amount of adsorbed oxygen on



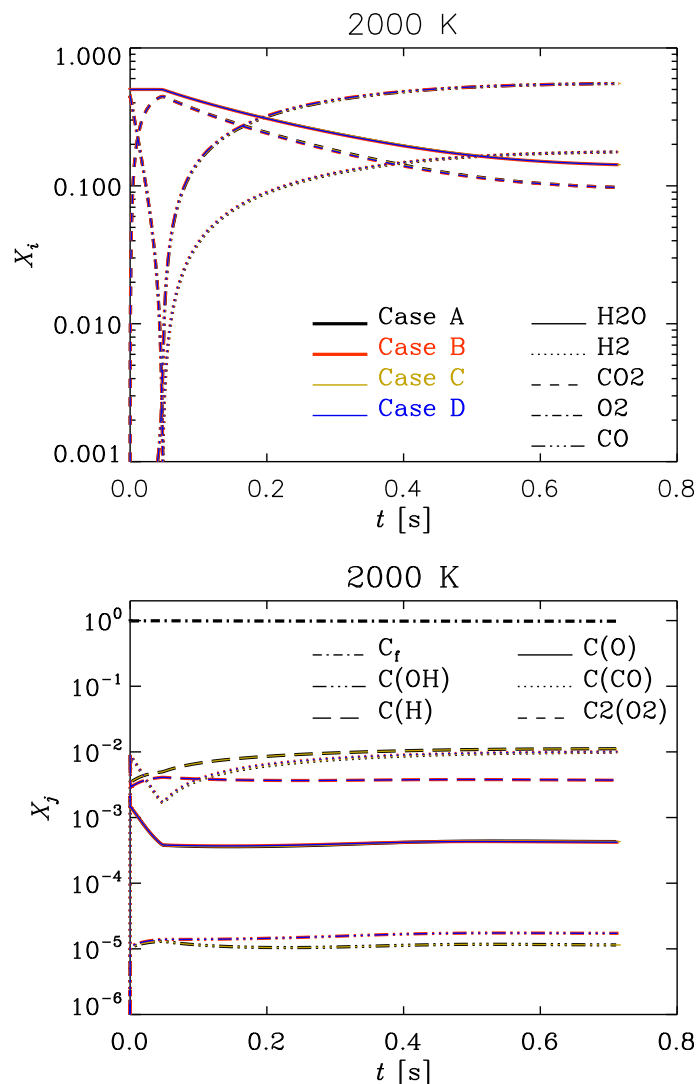


Figure 4: Gas phase species fraction  $X_i$  (top panel) and surface fraction  $X_j$  of adsorbed species (bottom panel) as a function of time at temperature of 2000 K.

the particle surface. This can be seen by comparing cases A and B in the lower panel of Fig. 4.

As a result of lower concentration of  $C(H)$ , reaction R8 slows down. This does not have an effect on the char conversion rate, since reaction R8 does not change the number of carbon atoms on the surface, but it does effect the net production rate of CO and HCO. This can be seen by comparing cases A and B in Fig. 5. Based on the above it may at first glance seem surprising that the molar concentrations of CO and HCO in the gas phase are still unchanged. This is however due to the fact that these species are converted through the homogeneous reactions in order to obtain

chemical equilibrium in the gas phase. At these high temperatures, gas phase chemical equilibrium is obtained at a time scale significantly shorter than the time scale for char conversion.

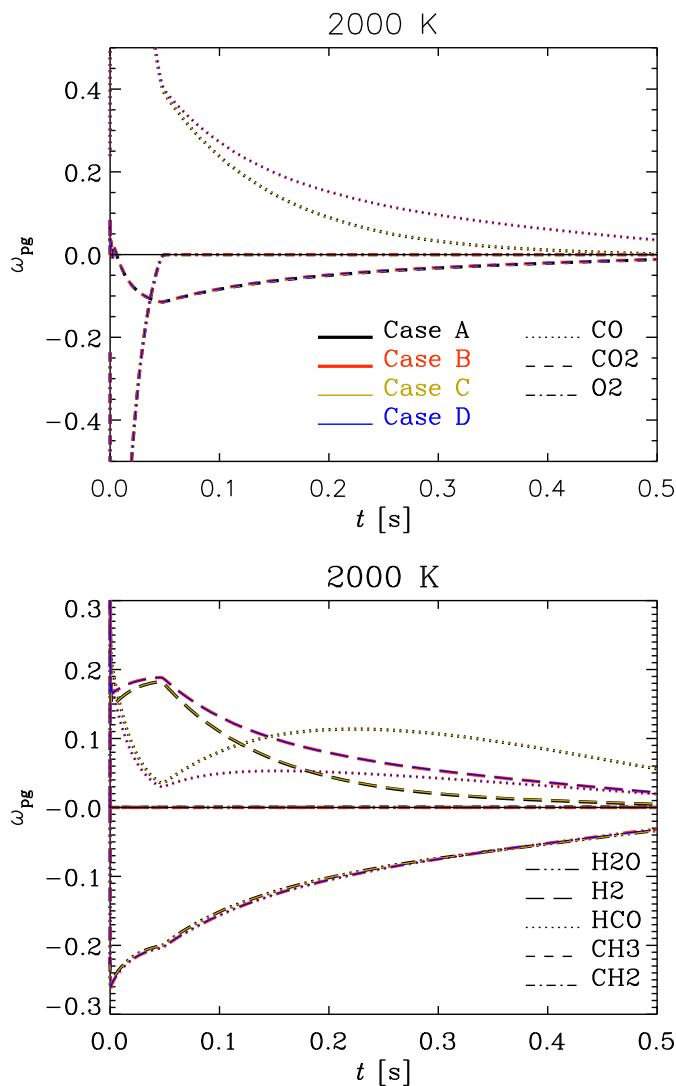


Figure 5: Species production rate  $\omega_{pg}$  due to the gas-to-particle reactions as a function of time at temperature of 2000 K.

In Fig. 4, the gas phase species concentration  $X_i$  and surface species concentration  $X_j$  as a function of time at a temperature of 2000 K is shown. The gas phase reaches chemical equilibrium since the difference between the fractions of each species can not be seen. The important difference is between cases A and B for the concentration of hydrogen adsorbed on the particle surface, which is higher in case A, since  $C(H)$  is not produced due to reaction R3b.

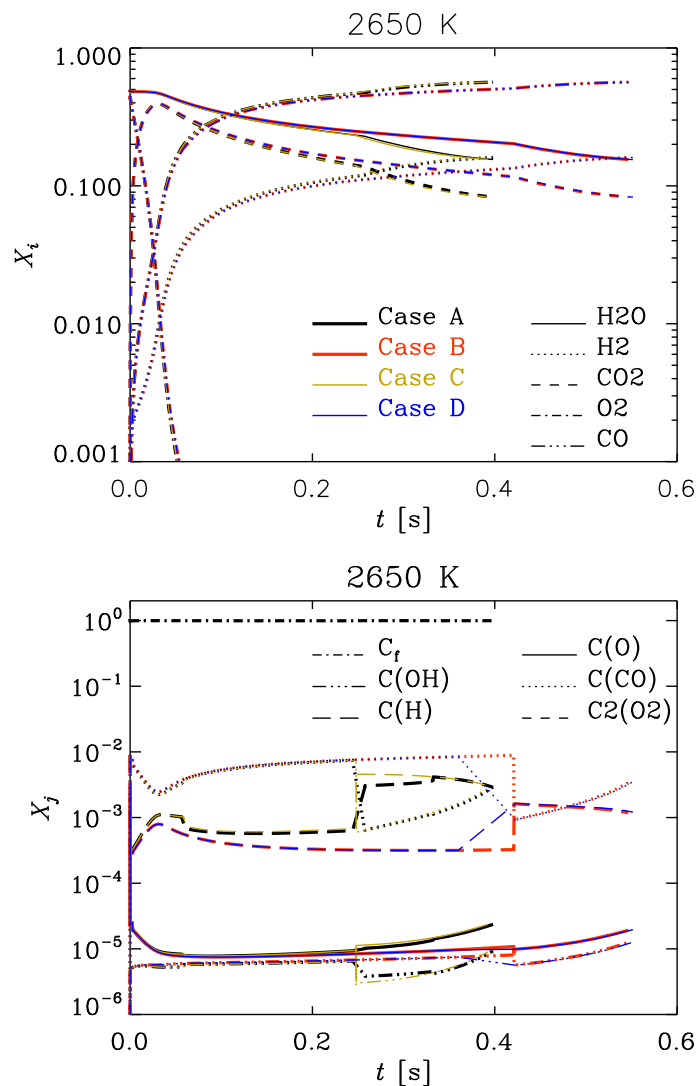


Figure 6: Gas phase species fraction  $X_i$  (top panel) and surface fraction  $X_j$  of adsorbed species (bottom panel) as a function of time at temperature of 2650 K.

By studying Fig. 6, it can be seen that several of the adsorbed species fractions make abrupt and seemingly unphysical jumps. Since smooth numerical results are no longer obtained, this indicates that a temperature of 2650 K is outside the temperature range for which the heterogeneous mechanism can be used. The reason for these jumps in adsorbed species fractions is probably that there exist two different solutions that both satisfy the governing equations at these rather extreme conditions. The numerical solver then ends up jumping between these two solutions, which yields the observed jumps in adsorbed species fractions.

## Gasification at very low temperatures

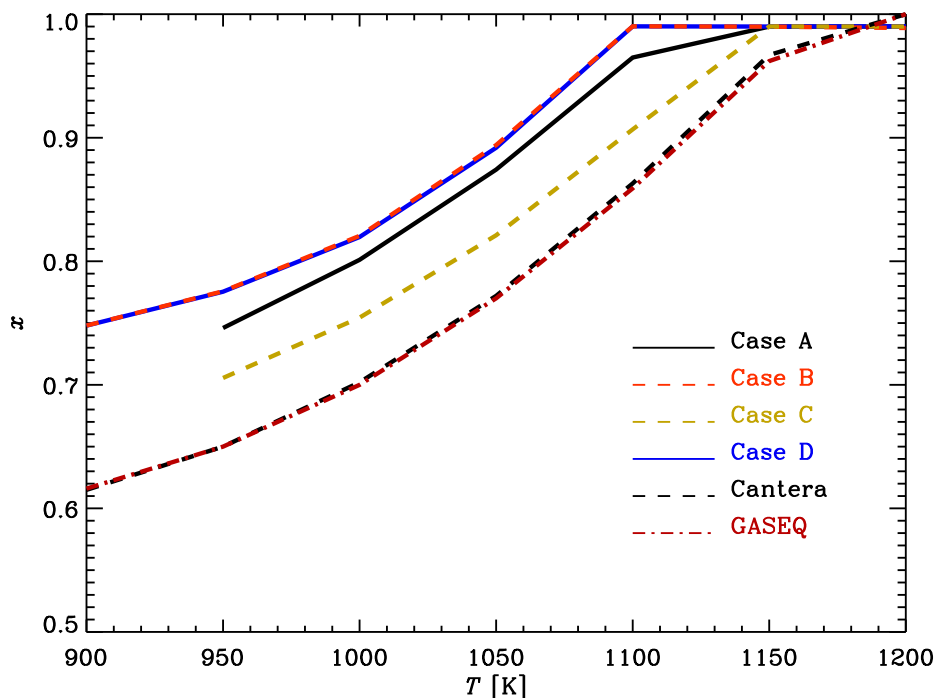


Figure 7: Conversion as a function of temperature for different cases and for two different equilibrium solvers.

At low temperatures, global chemical equilibrium dictates that full conversion of the char will not be obtained. For the conditions presented in Table 5, it is found that the char is fully converted for  $T > 1150$  K. Below this temperature, only a fraction of the char will be converted as  $t \rightarrow \infty$ .

The fraction of the char that gets converted is visualized by the solid lines in Fig. 7. Here it is seen that the amount of conversion decreases with temperature for all cases, but that the cases when reaction R3b is turned off always yield more conversion. The explanation for this is the same as before, namely that less adsorbed hydrogen on the surface yields more adsorbed oxygen, and hence more char conversion through reaction R4. The conversions shown here are obtained as time goes towards infinity, i.e. at chemical equilibrium. Hence, these results can be compared to results from chemical equilibrium solvers. Here, GASEQ<sup>20</sup> and Cantera<sup>21</sup> have been used to simulate the equilibrium condition. These results are visualized by the deep red dashed-dotted line and the black dashed line in Fig. 7. From this it is seen that the results for the two equilibrium solvers are

almost identical, as expected, and that the trends obtained from the equilibrium solvers are similar to what is found for cases A-D. The equilibrium solvers do, however, always yield a slightly lower conversion. Since one or more of the reactions are turned off in cases B-D, these cases are *not* expected to yield results similar to the equilibrium solvers. This is not true for case A, however. The reason for the discrepancy between the equilibrium solvers and case A is the fact that the equilibrium solvers do not take the adsorbed species into account. This means that the enthalpies and entropies of the char in the equilibrium solvers are not the same as in our main solver, hence the Gibbs free energy, and correspondingly also the equilibrium condition, is different.

## Summary

In this work, the newly developed detailed chemical kinetics model of Tilghman & Mitchell<sup>1</sup> has been used in order to study the mechanisms behind hydrogen inhibition and speed-up of char gasification. For the conditions studied here, it is clearly seen that hydrogen inhibition is found for  $T < 2000$  K, while for  $T > 2000$  K the hydrogen in the gas phase speeds up the char conversion. By studying the species reaction rates together with the individual rate of every single reaction, it is shown that hydrogen inhibition at low and intermediate temperatures is due to atomic hydrogen adsorbed on the char surface interacting with atomic oxygen on the surface to form an adsorbed *OH* molecule. The adsorbed *OH* molecule combines with another adsorbed hydrogen atom to form gaseous water. The outcome of this is that the adsorbed atomic oxygen, which would normally desorb as gaseous *CO* while removing a carbon atom from the surface, only takes part in the production of steam, which does not yield any char conversion, and hence the time to reach full conversion is increased due to the presence of hydrogen. This conclusion differs from the findings of Pineda & Chen<sup>4</sup> who found that hydrogen inhibition is mainly due to the blocking of active sites by adsorbed hydrogen. This discrepancy may be explained by the fact that adsorbed OH was not a part of their mechanism.

It has also been shown that at higher temperatures the presence of hydrogen results in a speed-

up of the char conversion. This is due primarily to reaction 6f, where adsorbed hydrogen reacts with steam to produce oxygen adsorbed on the surface. As a result of the higher concentration of  $C(O)$ , the process of removing carbon from the surface is faster.

## Acknowledgments

This work forms part of the CAMPS project supported by the Research Council of Norway (215707). The work has additionally been produced with support from the BIGCCS Centre, performed under the Norwegian Research Program Centres for Environment-Friendly Energy Research (FME). The author acknowledges the following partners for their contributions: Aker Solutions, ConocoPhillips, Gassco, Shell, Statoil, TOTAL, GDF SUEZ and the Research Council of Norway (193816/S60).

The research leading to these results has been received funding from the Polish-Norwegian Research Programme operated by the National Centre for Research and Development under the Norwegian Financial Mechanism 2009-2014 in the frame of Project Contract No Pol-Nor/232738/101/2014.

NELH also acknowledges the Research Council of Norway under the FRINATEK grant 231444.

## References

- (1) Tilghman, M. B & Mitchell, R. E.: 2015, "Coal and biomass char reactivities in gasification and combustion environments", *Combustion & Flame*, **162**, 3220-3235
- (2) Hecht, E. S., Shaddix, C. R., Molina, A. & Haynes, B. S.: 2011, "Effect of CO<sub>2</sub> gasification reaction on oxy-combustion of pulverized coal char", *Proc. Comb. Inst.*, **33**, 1699-1706
- (3) Haugen, N. E. L., Mitchell, R. E. & Tilghman, M. B.: 2014, "The conversion mode of a porous carbon particle during oxidation and gasification", *Combustion & Flame*, **161**, 612
- (4) Pineda, D. I. & Chen, J-Y: 2015 "Modeling hydrogen inhibition in gasification surface reactions", *Int. J. Hydrogen Energy*, **40**, 6059

- (5) Laurendeau, N. M.: 1978, "Heterogeneous kinetics of coal char gasification and combustion", *Prog. Energy Combust. Sci.*, **4**, 221-270
- (6) Gadsby, J., Hinshelwood, C. N. & Sykes, K. W.: 1946, "The Kinetics of the Reactions of the Steam-Carbon System", *Proc. Roy. Soc. A*, **187. A.**, 129-151
- (7) Johnstone, H. F., Chen, C.Y. & Scott, D.S.: 1952, "Kinetics of the steam-carbon reaction in porous graphite tubes", *Ind. Eng. Chem.*, **44(7)**, 1564-1569
- (8) Biederman, D.L., Miles, A.J., Vastola, F.J. & Walker Jr., P.L.: 1976, "Carbon-carbon dioxide reaction: kinetics at low pressures and hydrogen inhibition", *Carbon*, **14**, 351-356
- (9) Hüttinger, K.J. & Merdes, W.F.: 1992, "The carbon-steam reaction at elevated pressure: formations of product gases and hydrogen inhibitions", *Carbon*, **30(6)**, 883-894
- (10) Barrio, M., Gøbel, B., Risnes, H., Henriksen, U., Hustad, J.E. & Sørensen, L.H.: 2008, "Steam gasification of wood char and the effect of hydrogen inhibition on the chemical kinetics", *Progress in Thermochemical Biomass Conversion*
- (11) Mühlen, H-J, van Heek, K.H. & Jüntgen, H.:1985, "Kinetic studies of steam gasification of char in the presence of  $H_2$ ,  $CO_2$  and  $CO$ ", *Fuel*, **64(7)**, 944-949
- (12) Moilanen, A. & Mühlen, H-J: 1996, "Characterization of gasification reactivity of peat char in pressurized conditions effect of product gas inhibition and inorganic material", *Fuel*, **75(11)**, 1279-1285
- (13) Tay, H-L, Kajitani, S., Zhang, S. & Li, C-Z: 2014, "Inhibiting and other effects of hydrogen during gasification: Further insights from FT-Raman spectroscopy", *Fuel*, **116**, 1-6
- (14) Fushimi, C., Wada, T. & Tsutsumi, A.: 2011, "Inhibition of steam gasification of biomass char by hydrogen and tar", *Biomass and bioenergy*, **35(1)**, 179-185

- (15) Haugen, N. E. L., Mitchell, R. E. & Tilghman, M. B.: 2015, “A comprehensive model for char particle conversion in environments containing  $O_2$  and  $CO_2$ ”, *Combustion & Flame*, **162**, 1455-1463
- (16) Haynes, B. S.: 2001, “A turnover model for carbon reactivity I. development”, *Combustion & Flame*, **126**, 1421-1432
- (17) GRI-Mech 3.0 Homepage, August 2014. Available at [http://combustion.berkeley.edu/Combustion\\_Laboratory/gri-mech/overview.html](http://combustion.berkeley.edu/Combustion_Laboratory/gri-mech/overview.html).
- (18) Haugen, N. E. L. & Mitchell, R. E.: 2015, “Modeling radiation in particle clouds: On the importance of inter-particle radiation for pulverized solid fuel combustion” *Heat and Mass Transfer*, 51, 991-999
- (19) E. W. Thiele, *Ind. Eng. Chem* **31**, 916 (1939).
- (20) GASEQ; <http://www.gaseq.co.uk/>
- (21) Cantera; <https://en.wikipedia.org/wiki/Cantera>